EPJ Appl. Metamat. **5**, 7 (2018)

https://doi.org/10.1051/epjam/2018002

EPJ Applied Metamaterials

Available online at:
epjam.edp-open.org

Metamaterials'2017
Metamaterials and Novel Wave Phenomena: Theory, Design and Applications

REVIEW OPEN ACCESS

In pursuit of photo-induced magnetic and chiral microscopy★

Jinwei Zeng[1,*], Mohammad Kamandi[1], Mahsa Darvishzadeh-Varcheie[1], Mohammad Albooyeh[1], Mehdi Veysi[1], Caner Guclu[1], Mina Hanifeh[1], Mohsen Rajaei[1], Eric O. Potma[2], H.Kumar Wickramasinghe[1], and Filippo Capolino[1]

[1] University of California Irvine, Department of Electrical Engineering and Computer Science, 92697 Irvine, CA, USA
[2] University of California Irvine, Department of Chemistry, 92697 Irvine, CA, USA

Received: 10 November 2017 / Accepted: 24 January 2018

Abstract. Light-matter interactions enable the perception of specimen properties such as its shape and dimensions by measuring the subtle differences carried by an illuminating beam after interacting with the sample. However, major obstacles arise when the relevant properties of the specimen are weakly coupled to the incident beam, for example when measuring optical magnetism and chirality. To address this challenge we propose the idea of detecting such weakly-coupled properties of matter through the photo-induced force, aiming at developing photo-induced magnetic or chiral force microscopy. Here we review our pursuit consisting of the following steps: (1) Development of a theoretical blueprint of a magnetic nanoprobe to detect a magnetic dipole oscillating at an optical frequency when illuminated by an azimuthally polarized beam via the photo-induced magnetic force; (2) Conducting an experimental study using an azimuthally polarized beam to probe the near fields and axial magnetism of a Si disk magnetic nanoprobe, based on photo-induced force microscopy; (3) Extending the concept of force microscopy to probe chirality at the nanoscale, enabling enantiomeric detection of chiral molecules. Finally, we discuss difficulties and how they could be overcome, as well as our plans for future work.

Keywords: Photo-induced force microscopy / optical magnetism / chirality / magnetic force / chiral force / azimuthally polarized beam / structured light / nanostructures / magnetic nanoantenna / magnetic resonance

1 Introduction

Microscopy reveals material properties of the sample under study by observing its microscopic features. In addition to size and appearance, inexplicit material properties, such as refractive index and chemical composition, can be retrieved by monitoring changes induced by a probing beam that interacts with the sample. Naturally, this approach encounters some obstacles when the material properties of interest are weakly coupled to the incident beam, simply expressed by the question: "*how can we see things that do not interact with light?*"

Among the elusive material properties, we are particularly interested in photo-induced magnetism and chirality [1,2], due to their promising and fascinating implications, to name just a few: nanoscale magnetic imaging, magnetic tweezers and force microscopy, chirality detection, chiral force microscopy, magnetic spectroscopy, and spintronics, which have applications in material science, chemistry, and biology. However, both optical magnetism and chirality, which are related to the material's magnetic properties at optical frequencies, are typically weak and difficult to detect by conventional microscopy techniques that are typically based on the electric dipole response of the sample [2–6]. Moreover, the attempted nanoscale detection of such magnetic and chiral properties by conventional optical microscopy is especially difficult due to the diffraction limit.

In the realm of force microscopy, instead of "seeing" the specimen by detecting light at a distance, a special nanoprobe-tip is placed near the specimen to "feel" the photo-induced force between them. Force microscopy in general has unique merits superior to conventional optical microscopy. First and foremost, the tip-sample interaction force is always local, which decays fast as a function of increasing distance between the tip and the sample. Therefore, this force is intrinsically inert to background scattering noise which often plagues far field measurements, achieving a high signal-to-noise ratio (SNR). In addition, the resolution is high and limited only by the size of the scanning tip, achieving nanoscale resolution [7–9]. Moreover, the local force is a vector with both amplitude and direction, which can provide more information about the specimen than a simple scattering power-only measurement. Last but not least, the force can have different forms and origins, *which can be excited and harnessed* by a

* e-mail: jinweiz3@uci.edu
★ Invited Paper.

special probe-tip in force microscopy, thus revealing particular material properties. A perfect example of such force microscopy is photo-induced force microscopy (PiFM). PiFM usually uses a gold-coated tip for probing the photo-induced electromagnetic interaction force between the tip and the sample under external illumination, which is sensitive to the near-field light intensity distribution near the sample surface [7–11]. Compared to its precedent near-field scanning optical microscopy (NSOM), PiFM exhibits superior SNR and stability which are critical to study nanoscale light-matter interactions [7,8].

Similar to the concept of PiFM, which has thus far been used to probe electric dipole-type interactions in the tip-sample junction, we propose two new concepts of photo-induced force microscopy, namely photo-induced magnetic force microscopy (PiMFM) and photo-induced chiral force microscopy (PiCFM). Instead of using a gold-coated tip, PiMFM adopts a special magnetic probe-tip under suitable illumination to extract and detect the photo-induced magnetic force. Likewise, PiCFM may adopt either chiral or achiral tips, and use suitable illumination to detect the chirality-induced force, which reveals the chirality properties of the specimen, as we will discuss in this work.

We review our pursuit of PiMFM and PiCFM. It begins with a theoretical blueprint of PiMFM, which includes a magnetic nanoprobe that is illuminated by a focused azimuthally polarized beam (APB). In focus, the longitudinal magnetic field of the APB peaks on the beam axis while the electric field is vanishing [12–16]. When placed along the optical axis of the APB focal spot, the magnetic nanoprobe is able to selectively interact with the magnetic field [6,12–15]. Using this configuration, we characterize a tightly focused APB in the near-field by using PiFM to confirm the dominant magnetic field in the proximity of the optical axis [8]. Next, we discuss various designs of magnetic nanoprobes that support magnetic resonances [17–19] based on plasmonic and dielectric nano-structures [20–47]. We put particular emphasis on a Si nanodisk structure, and discuss PiFM measurements of the electric field distribution under APB illumination. Simultaneously, we propose a novel method and a roadmap that will enable chiral force microscopy with nanoscale resolution based on the interaction of a chiral sample with an achiral (plasmonic) scanning tip under structured light illumination [48–57]. Lastly, we discuss difficulties and future developments of this exciting area of research.

2 Blueprint of photo-induced magnetic force microscopy

Enabling detection of the magnetic part of the Lorentz force, $\hat{\mathbf{F}}\mathrm{m}(t) = \int_V \hat{\mathbf{J}} \times \hat{\mathbf{B}}\, dv$, where both current density $\hat{\mathbf{J}}$ and magnetic field $\hat{\mathbf{B}}$ oscillate at an optical frequency, involves two major tasks: first, designing a magnetic responsive probe that interacts with the magnetic field of light; and second, designing a light-matter interaction system that can distinguish the desired magnetic force from the electric counterpart, which is generally dominant. (The electric part $\hat{\mathbf{F}}_e(t) = \int_V \hat{\rho}\hat{\mathrm{E}}\, dv$ of the Lorentz force, where ρ is the volume charge density, is the directly measured photo-induced force in the PiFM [8–10].) The first task is accomplished by designing magnetically resonant nanostructures that enhance the optical magnetic field. The second task is accomplished by using an aligned APB illumination. Owing to the symmetry of the APBs, one can realize a time-harmonic magnetic-field dominant region where the electric field is polarized orthogonally to the propagation direction of the beam and is poised to circulate about the beam axis. Such circulating electric field generates a strong longitudinally polarized magnetic field on the beam axis where the electric field vanishes [13,14]. Using phasors, i.e., complex field vector associated to the time notation $\exp(-i\omega t)$, APBs are represented as a superposition of a right-handed circularly polarized beam with the OAM order of -1 and a left-handed circularly polarized beam with the OAM order of $+1$ as [14,16]

$$\mathbf{E} = \frac{-i\sqrt{2}}{2}\left(u_{-1,0}\hat{\mathbf{e}}_{\mathrm{RH}} - u_{1,0}\hat{\mathbf{e}}_{\mathrm{LH}}\right)e^{\mathrm{ikz}},$$

where $\hat{\mathbf{e}}_{\mathrm{RH}} = \left(\mathbf{1}_x + i\,\mathbf{1}_y\right)/\sqrt{2}$ and $\hat{\mathbf{e}}_{\mathrm{LH}} = \left(\mathbf{1}_x - i\,\mathbf{1}_y\right)/\sqrt{2}$ are, respectively, the right and left hand circularly polarized unit vectors, and the symbols $\mathbf{1}_{x,y}$ denote unit vectors. In the above equation, the electric field distributions with OAM orders $+1$ and -1, and radial order 0, are represented by $u_{\pm 1,0}$ whose expression is given in Equation (2) of Reference [14], expressed as Laguerre Gaussian beams solutions to the wave equation under paraxial approximation, and summarized here as

$$u_{\pm 1,\,0} = \frac{V}{\sqrt{\pi}}\frac{2\rho}{w^2}e^{-(\rho/w)^2\zeta}e^{-2i\,\mathrm{atan}(z/z_R)}e^{\pm i\phi},$$
$$w = w_0\sqrt{1+(z/z_R)^2},\ \zeta = 1 - iz/z_R,\ z_R = \pi w_0^2/\lambda.$$

Here V is the amplitude coefficient in unit of volts, ρ and z are the transverse and longitudinal observer position, respectively, and ϕ is the azimuthal angle. The field distribution of such a beam is shown in Figure 1a, where on the beam axis the magnetic field is maximum and the electric field vanishes.

We show next the concept of measuring the photo-induced magnetic force between a magnetically polarizable particle and a magnetic probe tip under APB illumination, based on simultaneously maintaining the rotational symmetry of the excitation signal (APB) and enhancing the magnetic field. Since natural magnetism fades at optical frequencies, an important aspect under investigation is the use of an engineered structure to provide artificial magnetism (i.e., magnetic dipoles) at optical frequencies that has become the focus of attention in recent years [20–33]. The building block in engineering artificial magnetism which is referred as magnetic nanoantenna in [17] varies from plasmonic structures [12,17,20–33] to high density nanosphere that exhibit a Mie-like magnetic resonance [34–47]. Magnetic nanoantennas, as nanoengineered structures to enhance the magnetic field at optical frequencies, host resonant modes with circulating electric currents or electric fields which give rise to magnetic dipoles oscillating at optical frequency. To this goal, we report two types of magnetic nanoantennas, dense

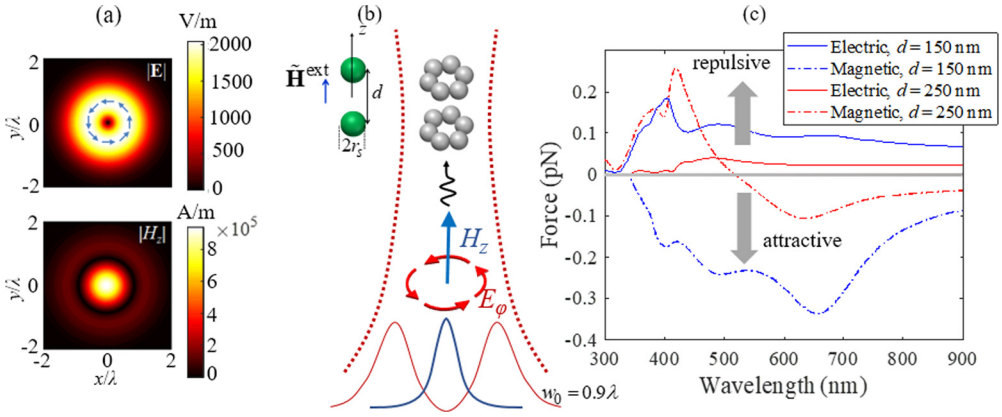

Fig. 1. (a) Total electric (top) and longitudinal magnetic (bottom) field maps of an APB with $w_0 = 0.9\,\lambda$ carrying 3 mW power [16]. (b) Schematic of an APB with longitudinal magnetic field illuminating two clusters of silver nanospheres or two high density dielectric spheres (e.g., two Si nanospheres). The two magnetic meta-atoms exert a near-field photo-induced force on each other [12,13]. (c) The electric and magnetic time-average forces acting on the top meta-atom (the clusters of plasmonic nanoparticles) located on the beam axis as function of wavelength. The APB has the beam waist parameter $w_0 = 0.9\,\lambda$ and 3 mW power. A significant attractive magnetic part of the Lorentz force is present [13].

dielectric nanospheres and circular clusters of plasmonic nanospheres as reliable candidates for magnetic nanoprobes as depicted in Figure 1b, c. Another strategy we are pursuing is based on using materials with strong magnetic dipolar transitions (based on some Lanthanides) that is not reported in this paper because it is currently under development.

A magnetic nanoprobe, consisting of a magnetic nanoantenna placed at a microscope scanning probe-tip, senses external *magnetic* fields in a very similar way as a gold-coated tip senses external *electric* field. At the resonance of the magnetic nanoantenna which is forming the magnetic nanoprobe, a magnetic dipole will be generated perpendicular to the circulating electric field or current. When a magnetic probe is used to sense the magnetic field (oscillating at optical frequency) generated by a sample nanostructure, at first glance it may be convenient to see the sample nanostructure as an oscillating magnetic dipole that generate a photo-induced "image" in the magnetic nanoprobe. More properly speaking the excitation of the magnetic nanoprobe is the result of near-field coupling between the nanoprobe and the sample nanostructure as explained in [13].

In [13], an estimate of the time-average force between the scanning magnetic nanoprobe and a magnetic sample was obtained by resorting to the canonical problem of calculation of the Lorentz force between two magnetically polarizable (at optical frequency) nanospheres, excited by external light. The time-average force between these two identical magnetically-interacting "meta-atoms", where the top one represents the scanning probe-tip and the bottom one represents a magnetic sample, is obtained from the formulas in Equation 2 of [13] as

$$\langle \hat{F} \rangle = \frac{\mu}{2} Re\left\{ m \left(\frac{\partial H_{z,\mathrm{loc}}}{\partial z} \right)^{*} \right\},$$

where $H_{z,\mathrm{loc}}$ represents local magnetic field polarized along the longitudinal direction acting on the top meta-atom, m represents the magnetic dipole moment of the top meta-atom oriented along z, and the asterisk symbol denotes complex conjugation. The local magnetic field $H_{z,\mathrm{loc}}$ is the sum of the magnetic field from the incident APB and the magnetic near-field arising from the bottom meta-atom. It is noteworthy that the magnetic near-field from the bottom meta-atom is dominant in both intensity and, especially, in the derivative of the intensity, when compared to that of the APB. Therefore the force acting on top meta-atom is dominated by the field generated by

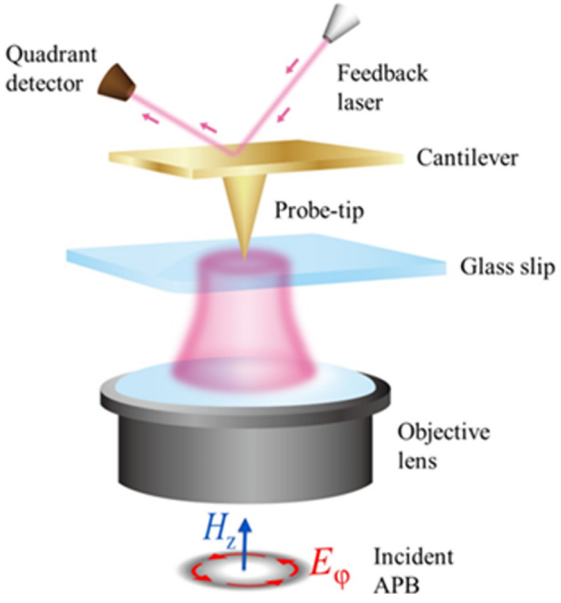

Fig. 2. The schematic of PiFM under sharply focused APB illumination. The tip-sample interaction force is detected by measuring the cantilever oscillation. The "sample" consists of the image of the tip in the glass substrate (as for the measurement in Fig. 3) or of a particle located on the substrate (as for the measurement in Fig. 4).

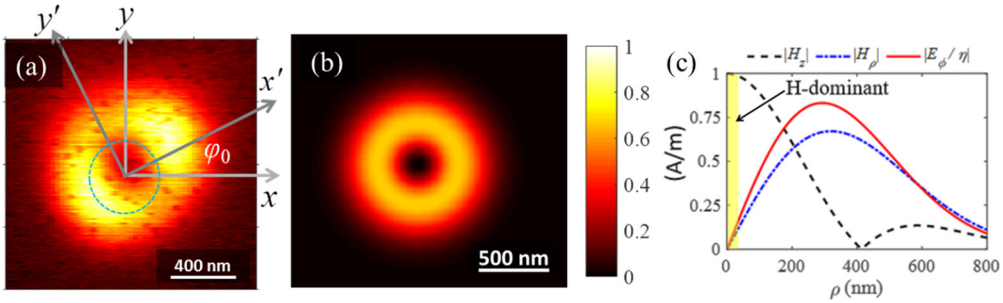

Fig. 3. (a) Measured force map of a sharply focused APB using PiFM, which exhibits a certain tip-induced anisotropy. (b) Corrected intensity distribution from the fitted model, removing tip anisotropy and noise [8]. (c) Retrieved electric and magnetic field of the sharply focused APB normalized to its maximum value. The highlighted magnetic dominant region is defined as when the normalized local field admittance $F_Y = \eta|H_z/E_\rho| > 10$, where η is the free space impedance [8,14,16].

the bottom meta-atom. Owing to the perfect symmetry of the two high density meta-atoms located on the axis, it is possible to show that the force is dominated by the interaction of the induced magnetic dipolar moments generated by the magnetic resonances. For the plasmonic cluster case the force between two meta-atoms is broken into two components, electrical and magnetic forces. Here we show in Figure 1d that the magnetic force is dominant and is of opposite polarity to the electrical one. Therefore, the time-average of the magnetic part of the Lorentz force $\hat{\mathbf{F}}\mathrm{m}(t) = \int_V \hat{\mathbf{J}} \times \hat{\mathbf{B}}\, dv$ is dominant compared to the time-average of the electric counterpart $\hat{\mathbf{F}}_e(t) = \int_V \hat{\rho}\hat{\mathbf{E}}\, dv$ under APB illumination.

3 Characterization of APB and Si disk magnetic nanoprobe by PiFM

The experimental realization of the proposed PiMFM starts from the characterization of the APB as the magnetic probing beam, together with the design, fabrication and characterization of a magnetic nanoprobe. In this section we show these two steps towards the construction of a PiMFM. We first use PiFM to measure the electric near-field distributions of the incident APB, and then measure the electric near field associated to the Si disk magnetic nanoprobe under APB illumination. We finally retrieve the corresponding magnetic field based on the measured electric field distribution, indirectly demonstrating the magnetic response in this structure.

Here we briefly review the mechanism of PiFM as our major instrument to investigate electric near-field distribution of a beam or a sample. As shown in Figure 2, the photo-induced force is detected by a modified AFM system, which uses an oscillating cantilever with probe-tip to feel the interaction force between the tip and the sample under external illumination. Note that here the total force exerted on the tip contains both photo-induced force and non-photo-induced force, and that the photo-induced force is selectively extracted by the lock-in mechanism [7,8,10]. The PiFM has both objective lens scanning and sample stage scanning mechanisms to measure the photo-induced force on the tip from the incident beam or the sample, respectively. The probe-tip in the PiFM is coated with a thin layer of gold (usually around 25 ~ 45-nm thick), and the gold grain on the tip-end acts as an electrically polarizable nanoparticle. Under external illumination, this plasmonic particle will be polarized as an electric dipole. When the tip dipole engages to a surface, the effect of the surface may be modeled as an imaging dipole created inside the surface, which, together with the tip-dipole, produces a photo-induced electric dipole-dipole interaction force. Under the assumption of perfectly symmetrical tip-dipole, this photo-induced force is proportional to the local electric field intensity [8,10]. However, for the realistic tip with azimuthal anisotropy, the measured photo-induced force will exhibit certain tip-induced asymmetry. Such an error is corrected by calibration with the incident APB [8]. The incident APB is azimuthally symmetric with uniform phase distribution at its transverse plane; besides, it has no longitudinal electric field component regardless of sharp focusing or not [14]. This simplicity makes the APB an ideal candidate for calibration standard, in addition to its interesting magnetic probing feature introduced previously. The force map of sharply focused APB is measured by PiFM with a scanning objective lens, i.e., by translating the APB, shown in Figure 3a. Then we resort to a theoretical model of the APB to fit the measured electric dipole-dipole interaction force, and eventually retrieve the electric and magnetic field distribution [8] as shown in Figure 3b. We define the magnetic dominant region where the normalized local field admittance defined as $F_Y = \eta|H_z/E_\rho|$ is larger than 10, and this is shown in Figure 3c. Note any $F_Y > 1$ implies that the structured light has a stronger local magnetic field, normalized to the electric field, than that of a plane wave [14,16], and thus it is more suitable to test material's magnetic properties than a plane wave since material's response to electric field is usually stronger than its response to magnetic field.

Next, we design, fabricate and characterize a Si disk as a simple but effective magnetic nanoprobe. Indeed the Si disk as a high-index dielectric supports a Mie-type magnetic resonance [38–47]. We have chosen the Si disk structure to proceed with the experimental development due to two major reasons. First, when compared to the plasmonic-cluster magnetic probe introduced earlier, that requires an extremely fine detailed structure, the Si disk structure exhibits great convenience and simplicity in both design and fabrication. Moreover, dielectric materials, like Si, usually exhibit less loss than plasmonic materials like gold,

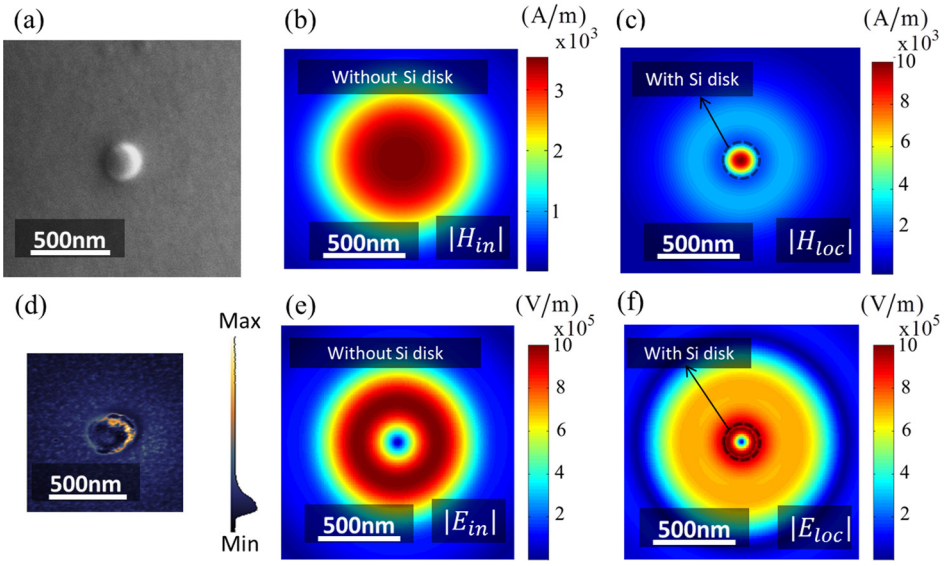

Fig. 4. (a) The SEM image of the fabricated Si disk on a glass slip. (b) The simulated magnitude of the magnetic field profile of the incident APB without Si disk, and (c) in presence of the Si disk, both observed in a transverse cross section 5 nm above the disk upper boundary. (d) Preliminary result of a force map of the Si disk exposed to the incident APB measured by PiFM. Force is proportional to the magnitude square of the illuminating electric field [8]. (e) Simulated magnitude of the electric field profile of the incident APB without the presence of the Si disk, and (f) in presence of the Si disk, still observed in a transverse cross section 5 nm above the disk upper boundary.

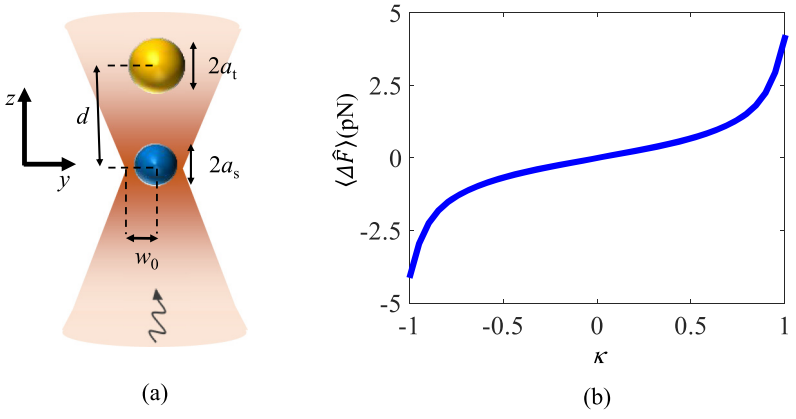

Fig. 5. (a) Schematic of the photo-induced chiral force microscopy (PiCFM) concept, enabling the detection of chirality of a sample based on differential force measurement. (b) Photo-induced differential force exerted on the tip (represented by the yellow nanosphere), from two incident scenarios of RCP and LCP light versus chirality parameter of the sample [48]. Differential time-average force can be positive or negative, depending on the chiral parameter κ of the material in the sample (represented by the blue sphere).

which is also a critical factor in our delicate optical system since losses would compromise the strength of the resulting magnetic dipole. Here we design the Si disk with 80-nm height and 200-nm diameter to magnetically resonate at the free-space wavelength of 670 nm, assumed to be immersed in a homogeneous medium with relative electric permittivity of 2.25. The Si disk is fabricated by first depositing a uniform Si film about 80-nm thick on a glass cover slip, then the FIB is used to remove most of the film, leaving the standing disk. The SEM of the fabricated Si disk, is shown in Figure 4a. The electromagnetic response of this structure is studied under incident APB oscillating at the same frequency as the resonance frequency of the disk. The beam waist parameter of the incident APB is set as $w_0 = 469$ nm, and the incident power is 1 mW. Electromagnetic simulations are carried out using the finite element method implemented in CST Microwave Studio. Figure 4b, c and Figure 4e, f show the transverse cross section of the magnetic and electric field distributions at 5 nm above the upper boundary of the disk, in presence (c,f) and in absence (b,e) of the disk, respectively. According to Figure 4c and f, the maximum of magnetic field happens along the disk axis while the electric field is maximum around the edge of the disk. The magnetic field enhancement at the disk axis, defined as the local magnetic field divided by the incident magnetic field, indicates this structure is magnetic responsive.

The experimental result is obtained by placing the Si disk into the PiFM with an incident APB to perform PiFM characterization. After the incident APB is configured as described previously, the tip is aligned to the center of the beam and the stage scan is performed to acquire the electric field distribution map in Figure 4d that shows a donut shape, which agrees with the simulated electric field distribution, and indirectly demonstrates the magnetic response of this structure as designed. The measured electric field distribution shows certain asymmetry, which to our understanding is originated from the combination of an asymmetric fabricated disk, an asymmetric realistic tip-end, and an imperfect tip and beam axis alignment.

4 Photo-induced chiral force and microscopy

Detection and characterization of chiral structures as one of the fundamental constituents of biomolecules is a crucial task in chemical and biological applications [49–53]. Conventionally, chiroptical techniques such as circular dichroism (CD) are exploited to identify the material chirality which require substantial amount of sample material with a high concentration. This is because the chirality effect as an indirect electric to magnetic coupling between incident light and sample material is typically very weak compared to the electric property which is a direct coupling between the electric part of the incident light and the sample's electric properties [54–57]. Therefore, the observation of chirality might be masked under the electric properties in chiroptical techniques if a substantial amount of material is not provided. Consequently, these techniques are not suitable for detection of chirality for nanoscale samples. In this section, we introduce a new technique based on force microscopy for enantiomeric detection of nanoscale chiral samples. In our proposed technique, we employ the PiFM platform with circularly polarized (CP) beam illumination and measure the electromagnetic force that is applied to the cantilever tip in the vicinity of the sample. Specifically, we consider the differential force in the longitudinal direction, i.e. the z-axis in Figure 5a, between two CP illuminations with opposite handedness. For an achiral sample, the exerted time-average force on the tip is equal in both cases, however, for chiral samples, thanks to its optical activity, the difference between the exerted force on the tip for these two different illuminations does not vanish and reads

$$\langle \Delta \hat{F} \rangle = \langle \hat{F}_z^{\mathrm{RCP}} \rangle - \langle \hat{F}_z^{\mathrm{LCP}} \rangle,$$

in which $\langle \hat{F}_z^{\mathrm{RCP}} \rangle$ and $\langle \hat{F}_z^{\mathrm{LCP}} \rangle$ are the exerted time-average force on the tip for the two excitation scenarios with RCP and LCP incident beams, respectively. It has been shown in [48] that this differential time-average force linearly depends on the electric polarizability of the tip α_t^{ee}, magneto-electric polarizability of the sample α_s^{em} and the intensity of the beam $|\mathbf{E}_0|^2$, i.e.,

$$\langle \Delta \hat{F} \rangle \approx -\frac{3|\mathrm{E}_0|^2}{4\pi\sqrt{\varepsilon_0\mu_0}d^4} Im\{\alpha_t^{\mathrm{ee}}(\alpha_s^{\mathrm{em}})^*\},$$

where d is the distance between the center of the sample and the center of the tip. Therefore, the choice of the tip material and its shape plays an important role in the enhancement of the observed quantity $\langle \Delta \hat{F} \rangle$ and, hence, the chirality detection of nanoscale samples with small chirality parameter. Thanks to the presence of a plasmonic tip at the vicinity of the chiral sample, our technique will bring the opportunity to measure small values of chirality in nanoscale samples. To illustrate the capability of our proposed methodology in detecting chirality, we consider an example where the sample and the tip are both considered as spheres with equal radii of $r_s = r_t = 65\,nm$ and are at a distance to form a particle-to-particle distance of $d = 140\,\mathrm{nm}$ (see Fig. 5a). We assume the plasmonic tip is made of gold as introduced before in order to enhance the exerted force on the tip. Furthermore, we consider the relative permittivity of the sample to be $\varepsilon_s = 2.5$. The incident light is assumed to be circularly polarized propagating along the z-direction with Gaussian distribution with $w_0 = 0.7\,\lambda_0$ beam waist, and 1 mW power at wavelength of $\lambda_0 = 520\,\mathrm{nm}$. The sample is located at the center of the minimum waist of the Gaussian beam (where the field is strongest) and is made of chiral inclusions described by the chirality parameter κ that here varies from -1 to 1. We have calculated the z-component of the exerted force on the tip versus the chirality parameter κ, for both RCP and LCP illuminations and have illustrated the result in Figure 5b. This result clearly shows that for an achiral sample ($\kappa = 0$), the induced force on the tip is equal for RCP and LCP incidences cases, i.e., the differential force ΔF vanishes. However, as we increase the amplitude of the chirality parameter of the sample, the differential force becomes more obvious, in the order of piconewtons (Fig. 5b) which is measurable with the present force microscopes [48,58]. Note also the sign of the differential force depends on the sign (i.e., the handedness) of the chiral parameter κ of the sample material.

As a conclusion of this part, it is worth mentioning that compared to conventional chiroptical measurement methods such as CD that takes average of far-field scattering of molecules in a solution which requires sub-milliliter volumes with micromolar molecular concentration, the proposed photo-induced chiral force microscopy exploits near-field information which is enhanced by the presence of a plasmonic tip and offers a fundamentally new measurement paradigm for chirality detection of nanoscale samples.

5 Challenges, Visions, and roadmaps forward

We have summarized some of the achievements towards our goal of experimental demonstration of the PiMFM and PiCFM concepts. One major challenge is the fabrication of the special probe tips required for PiMFM and PiCFM purposes. While force microscopy provides

exceptional opportunities for high SNR, resolution, and exclusive excitation of photo-induced magnetic or chiral force, this system is also delicate due to the tiny and fragile microscopy probe-tip. For the proposed PiMFM and PiCFM, their probe-tips are required with special materials, shapes, and nano-scaled sizes. Direct fabrication methods including focused ion beam (FIB) or electron beam lithography (EBL) are tricky, because when the tip-end is zoomed-in and focused by scanning electron or ion beams, it could be damaged immediately. Therefore, focusing and alignment during these fabrication methods must be performed fast and accurately for a high success rate.

Alternatively, ad-hoc probe-tips for PiMFM or PiCFM can be fabricated separately and then "picked-up" and attached to the cantilever. Lanthanides and DNA have the capability to interact and contribute to optical magnetism and chirality [2,5,6,59–65], therefore nanostructures incorporating these materials can serve as ideal probe-tips for optical magnetism or chirality detection purposes. Following this approach, a challenge is in firmly attaching such particles to the ideal position on the cantilever in a stable way. We are currently investigating different mechanism to attach particles on AFM tip, including chemical bonding, gold-gold bonding etc.

Once the new probe-tips will be successfully implemented into a force microscopy system, other challenges should be resolved including optimizing cantilever oscillation amplitude, tip engaging setpoint, drive and detection frequency, and selection of the cantilevers, etc. A fundamental aspect for the success of such new microscopy systems is the use of sharply focused structured light to select the proper physical properties that give rise to local near-field interaction forces.

Microscopy of optical magnetism and chirality are two great examples of promising applications offered by force microscopy. We emphasize that similar ideas can be extended to inspecting other interesting properties of material or light by playing with combinations of structured light and different kinds of nanoprobes. For examples, we can detect photo-induced orbital force on a sample, induced by optical vortices with orbital angular momentum [66,67]; or we could investigate also the lateral force [68] in addition of the longitudinal force, induced by chiral particles under chiral light. We could look into the local field distribution of metamaterials or metasurfaces in special resonances and verify their origins. etc. All these are open questions and exciting possibilities that await explorations. We envision that force microscopy will gain fundamental recognition as an unparalleled multi-purpose tools for optical near-field characterization in the future of nano-photonics.

Funding

W. M. Keck Foundation (USA).

NSF Center for Chemical Innovation – Chemistry at the Space-Time Limit (CHE-1414466).

The authors are grateful to CST Simulation Technology AG for the simulation tool CST Microwave Studio that was instrumental in this analysis.

References

1. F. Monticone, A. Alù, The quest for optical magnetism: from split-ring resonators to plasmonic nanoparticles and nanoclusters, J. Mater. Chem. C **2**, 9059 (2014)
2. L.D. Barron, An introduction to chirality at the nanoscale, in: D.B. Ambilino (Ed.), Chirality at the Nanoscale: Nanoparticles, Surfaces, Materials and More Wiley-VCH, Weinheim, Germany, 2009
3. M. Burresi, D. van Oosten, T. Kampfrath, H. Schoenmaker, R. Heideman, A. Leinse, L. Kuipers, Probing the magnetic field of light at optical frequencies, Science **326**, 550 (2009)
4. H. Giessen, R. Vogelgesang, Glimpsing the weak magnetic field of light, Science **326**, 529 (2009)
5. T.H. Taminiau, S. Karaveli, N.F. van Hulst, R. Zia, Quantifying the magnetic nature of light emission, Nat. Commun. **3**, 979 (2012)
6. M. Kasperczyk, S. Person, D. Ananias, L.D. Carlos, L. Novotny, Excitation of magnetic dipole transitions at optical frequencies, Phys. Rev. Lett. **114**, 163903 (2015)
7. D. Nowak, W. Morrison, H.K. Wickramasinghe, J. Jahng, E. O. Potma, L. Wan, R. Ruiz, T.R. Albrecht, K. Schmidt, J. Frommer, D.P. Sanders, Nanoscale chemical imaging by photoinduced force microscopy, Sci. Adv. **2**, e1501571 (2016)
8. J. Zeng, F. Huang, C. Guclu, M. Veysi, M. Albooyeh, H.K. Wickramasinghe, F. Capolino, Sharply focused azimuthally polarized beams with magnetic dominance: near- field characterization at nanoscale by photoinduced force microscopy, ACS Photonics (2017) DOI: 10.1021/acsphotonics.7b00816
9. I. Rajapaksa, K. Uenal, H.K. Wickramasinghe, Image force microscopy of molecular resonance: a microscope principle, Appl. Phys. Lett. **97**, 073121 (2010)
10. F. Huang, V.A. Tamma, Z. Mardy, J. Burdett, H.K. Wickramasinghe, Imaging nanoscale electromagnetic near-field distributions using optical forces, Sci. Rep. **5**, 10610 (2015)
11. J. Jahng, J. Brocious, D.A. Fishman, F. Huang, X. Li, V.A. Tamma, H.K. Wickramasinghe, E.O. Potma, Gradient and scattering forces in photoinduced force microscopy, Phys. Rev. B. **90**, 155417 (2014)
12. C. Guclu, M. Veysi, F. Capolino, Photoinduced magnetic nanoprobe excited by an azimuthally polarized vector beam, ACS Photonics **3**, 2049 (2016)
13. C. Guclu, V.A. Tamma, H.K. Wickramasinghe, F. Capolino, Photoinduced magnetic force between nanostructures, Phys. Rev. B. **92**, 235111 (2015)
14. M. Veysi, C. Guclu, F. Capolino, Focused azimuthally polarized vector beam and spatial magnetic resolution below the diffraction limit, J. Opt. Soc. Am. B. **33**, 2265 (2016)
15. P. Wozniak, P. Banzer, G. Leuchs, Selective switching of individual multipole resonances in single dielectric nanoparticles, Laser Photon. Rev. **9**, 231 (2015)
16. M. Veysi, C. Guclu, F. Capolino, Vortex beams with strong longitudinally polarized magnetic field and their generation by using metasurfaces, J. Opt. Soc. Am. B. **32**, 345 (2015)

17. M. Darvishzadeh-Varcheie, C. Guclu, F. Capolino, Magnetic nanoantennas made of plasmonic nanoclusters for photoinduced magnetic field enhancement, Phys. Rev. Appl. **8**, 024033 (2017)
18. C. Guclu, M. Veysi, M. Darvishzadeh-Varcheie, F. Capolino, Proceedings of conference on Lasers and Electro-Optics, Artificial Magnetism via Nanoantennas under Azimuthally Polarized Vector Beam Illumination, OSA Technical Digest, 2016
19. C. Guclu, M. Veysi, M. Darvishzadeh-Vercheie, F. Capolino, Optical nanoantennas as magnetic nanoprobes for enhancing light-matter interaction, Proceedings of the 2016 10th International Congress on Advanced Electromagnetic Materials in Microwaves and Optics, Chania, 2016, pp. 391–393
20. G Dolling, C. Enkrich, M. Wegener, J.F. Zhou, C.M. Soukoulis, S. Linden, Cut-wire pairs and plate pairs as magnetic atoms for optical metamaterials, Opt. Lett. **30**, 3198 (2005)
21. V.M. Shalaev, W. Cai, U.K. Chettiar, H.-K. Yuan, A.K. Sarychev, V.P. Drachev, A.V. Kildishev, Negative index of refraction in optical metamaterials, Opt. Lett. **30**, 3356 (2005)
22. A. Alu, A. Salandrino, N. Engheta, Negative effective permeability and left-handed materials at optical frequencies, Opt. Express **14**, 1557 (2006)
23. A. Alu, N. Negheta, The quest for magnetic plasmons at optical frequencies, Opt. Express **17**, 5723 (2009)
24. S. Campione, C. Guclu, R. Ragan, F. Capolino, Enhanced magnetic and electric fields via Fano resonances in metasurfaces of circular clusters of plasmonic nanoparticles, ACS Photonics **1**, 254 (2014)
25. C.R. Simovski, S.A. Tretyakov, Model of isotropic resonant magnetism in the visible range based on core-shell clusters, Phys. Rev. B **79**, 045111 (2009)
26. D.K. Morits, C.R. Simovski, Negative effective permeability at optical frequencies produced by rings of plasmonic dimers, Phys. Rev. B **81**, 205112 (2010)
27. A. Vallecchi, M. Albani, F. Capolino, Collective electric and magnetic plasmonic resonances in spherical nanoclusters, Opt. Express **19**, 2754 (2011)
28. A. Vallecchi, M. Albani, F. Capolino, Effect of irregularities of nanosatellites position and size on collective electric and magnetic plasmonic resonances in spherical nanoclusters, Opt. Express **21**, 7667 (2013)
29. A. Vallecchi, S. Campione, F. Capolino, Symmetric and antisymmetric resonances in a pair of metal-dielectric nanoshells: tunability and closed-form formulas, J. Nanophoton. **4**, 041577 (2010)
30. Z. Qian, S.P. Hastings, C. Li, B. Edward, C.K. McGinn, N. Engheta, Z. Fakhraai, S.-J. Park, Raspberry-like metamolecules exhibiting strong magnetic resonances", ACS Nano **9**, 1263 (2015)
31. B. Luk'yanchuk, N.I. Zheludev, S.A. Maier, N.J. Halas, P. Nordlander, H. Giessen, C.T. Chong, The Fano resonance in plasmonic nanostructures and metamaterials, Nat. Mater. **9**, 707 (2010)
32. S.N. Sheikholeslami, A. García-Etxarri, J.A. Dionne, Controlling the interplay of electric and magnetic modes via Fano-like plasmon resonances, Nano Lett. **11**, 3927 (2011)
33. V. Ponsinet, P. Barois, S.M. Gali, P. Richetti, J.B. Salmon, A. Vallecchi, M. Albani, A. Le Beulze, S. Gomez-Grana, E. Duguet, S. Mornet, M. Treguer-Delapierre, Resonant isotropic optical magnetism of plasmonic nanoclusters in visible light, Phys. Rev. B **92**, 220414 (2015)
34. C. Enkrich, M. Wegener, S. Linden, S. Burger, L. Zschiedrich, F. Schmidt, J.F. Zhou, T. Koschny, C.M. Soukoulis, Magnetic metamaterials at telecommunication and visible frequencies, Phys. Rev. Lett. **95**, 203901 (2005)
35. T.D. Corrigan, P.W. Kolb, A.B. Sushkov, H.D. Drew, D.C. Schmadel, R.J. Phaneuf, Optical plasmonic resonances in split-ring resonator structures: an improved LC model, Opt. Express **16**, 19850 (2008)
36. S. Mühlig, A. Cunningham, S. Scheeler, C. Pacholski, T. Bürgi, C. Rockstuhl, F. Lederer, Self-assembled plasmonic core-shell clusters with an isotropic magnetic dipole response in the visible range, ACS Nano **5**, 6586 (2011)
37. F. Shafiei, F. Monticone, K.Q. Le, X.-X. Liu, T. Hartsfield, A. Alù, X. Li, A subwavelength plasmonic metamolecule exhibiting magnetic-based optical Fano resonance, Nat. Nanotechnol. **8**, 95 (2013)
38. R.S. Savelev, S.V. Makarov, A.E. Krasnok, P.A. Belov, From optical magnetic resonance to dielectric nanophotonics (A review), Opt. Spectrosc. **119**, 551 (2015)
39. A.I. Kuznetsov, A. Miroshnichenko, H.Y. Fu, J. Zhang, B. Luk'yanchuk, Magnetic light, Sci. Rep. **2**, 492 (2012)
40. D. Permyakov, I. Sinev, D. Markovich, P. Ginzburg, A. Samusev, P. Belov, V. Valuckas, A.I. Kuznetsov, B.S. Luk'yanchuk, A.E. Miroshnichenko, D.N. Neshev, Y. Kivshar, Probing magnetic and electric optical responses of silicon nanoparticles, Appl. Phys. Lett. **106**, 171110 (2015)
41. I. Staude, A.E. Miroshnichenko, M. Decker, N.T. Fofang, S. Liu, E. Gonzales, J. Dominguez, T.S. Luk, D.N. Neshev, I. Brener, Y. Kivshar, Tailoring directional scattering through magnetic and electric resonances in subwavelength silicon nanodisks, ACS Nano 7, 7824 (2013)
42. A.E. Krasnok, A.E. Miroshnichenko, P.A. Belov, Y.S. Kivshar, All-dielectric optical nanoantennas, Opt. Express **20**, 20599 (2012)
43. A.I. Kuznetsov, A.E. Miroshnichenko, M.L. Brongersma, Y. S. Kivshar, B. Luk'yanchuk, Optically resonant dielectric nanostructures, Science **354**, 2472 (2016)
44. S. Campione, S. Lannebere, A. Aradian, M. Albani, F. Capolino, Complex modes and artificial magnetism in three-dimensional periodic arrays of titanium dioxide microspheres at millimeter waves, J. Opt. Soc. Am. B **29**, 1697 (2012)
45. R. Alaee, M. Albooyeh, M. Yazdi, N. Komjani, C. Simovski, F. Lederer, C. Rockstuhl, Magnetoelectric coupling in nonidentical plasmonic nanoparticles: theory and applications, Phys. Rev. B **91**, 115119 (2015)
46. R. Alaee, M. Albooyeh, A. Rahimzadegan, M.S. Mirmoosa, Y.S. Kivshar, C. Rockstuhl, All-dielectric reciprocal bianisotropic nanoparticles, Phys. Rev. B **92**, 245130 (2015)
47. R. Alaee, M. Albooyeh, S. Tretyakov, C. Rockstuhl, Phase-change material-based nanoantennas with tunable radiation patterns, Opt. Lett. **41**, 4099 (2016)
48. M. Kamandi, M. Albooyeh, C. Guclu, M. Veysi, J. Zeng, H.K. Wickramasinghe, F. Capolino, Enantio-specific detection of chiral nano-samples using photo-induced force, Phys. Rev. Appl. **8**, 064010 (2017)

49. A.O. Govorov, Z. Fan, P. Hernandez, J.M. Slocik, R.R. Naik, Theory of circular dichroism of nanomaterials comprising chiral molecules and nanocrystals: plasmon enhancement, dipole interactions, and dielectric effects, Nano Lett. **10**, 1374 (2010)
50. A.O. Govorov, Plasmon-induced circular dichroism of a chiral molecule in the vicinity of metal nanocrystals. application to various geometries, J. Phys. Chem. C **115**, 7914 (2011)
51. J.M. Slocik, A.O. Govorov, R.R. Naik, Plasmonic circular dichroism of peptide-functionalized gold nanoparticles, Nano Lett. **11**, 701 (2011)
52. F. Lu, Y. Tian, M. Liu, D. Su, H. Zhang, A.O. Govorov, O. Gang, Discrete nanocubes as plasmonic reporters of molecular chirality, Nano Lett. **13**, 3145 (2013)
53. Y. Zhao, A.A.E. Saleh, J.A. Dionne, Enantioselective optical trapping of chiral nanoparticles with plasmonic tweezers, ACS Photonics **3**, 304 (2016)
54. N.J. Greenfield, Using circular dichroism spectra to estimate protein secondary structure, Nat. Photonics **1**, 2876 (2006)
55. R. Tullius, A.S. Karimullah, M. Rodier, B. Fitzpatrick, N. Gadegaard, L.D. Barron, V.M. Rotello, G. Cooke, A. Lapthorn, M. Kadodwala, Superchiral spectroscopy: detection of protein higher order hierarchical structure with chiral plasmonic nanostructures, J. Am. Chem. Soc. **137**, 8380 (2015)
56. Y. Zhao, A.N. Askarpour, L. Sun, J. Shi, X. Li, A. Alù, Chirality detection of enantiomers using twisted optical metamaterials, Nat. Commun. **8**, 14180 (2017)
57. S.M. Kelly, T.J. Jess, N.C. Price, How to study proteins by circular dichroism, Biochim. Biophys. Acta **1751**, 119 (2005)
58. Y. Martin, C.C. Williams, H.K. Wickramasinghe, Atomic force microscope-force mapping and profiling on a sub 100-Å scale, J. Appl. Phys. **61**, 4723 (1987)
59. R. Hussain, S.S. Kruk, C.E. Bonner, M.A. Noginov, I. Staude, Y.S. Kivshar, N. Nogionva, D.N. Neshev, Enhancing Eu 3 + magnetic dipole emission by resonant plasmonic nanostructures, Opt. Lett. **40**, 1659 (2015)
60. W.T. Carnall, P.R. Fields, B.G. Wybourne, Spectral intensities of the trivalent lanthanides and actinides in solution. I. Pr3+, Nd3+, Er3+, Tm3+, and Yb3+, J. Chem. Phys. **42**, 3797 (1965)
61. W.T. Carnall, P.R. Fields, K. Rajnak, Spectral intensities of the trivalent lanthanides and actinides in solution. II. Pm3+, Sm3+, Eu3+, Gd3+, Tb3+, Dy3+, and Ho3+, J. Chem. Phys. **49**, 4412 (1968)
62. C.M. Dodson, R. Zia, Magnetic dipole and electric quadrupole transitions in the trivalent lanthanide series: calculated emission rates and oscillator strengths, Phys. Rev. B **86**, 125102 (2012)
63. H. Kurzen, L. Bovigny, C. Bulloni, C. Daul, Electronic structure and magnetic properties of lanthanide 3+ cations, Chem. Phys. Lett. **574**, 129 (2013)
64. D. Li, M. Jiang, S. Cueff, C.M. Dodson, S. Karaveli, R. Zia, Quantifying and controlling the magnetic dipole contribution to 1.5 μm light emission in erbium-doped yttrium oxide, Phys. Rev. B **89**, 161409 (2014)
65. K. Binnemans, Interpretation of europium (III) spectra, Coordin. Chem. Rev. **295**, 1 (2015)
66. C.T. Schmiegelow, F. Schmidt-Kaler, Light with orbital angular momentum interacting with trapped ions, Eur. Phys. J. D **66**, 157 (2012)
67. N. Litchinitser, Structured light meets structured matter, Science **337**, 1054 (2012)
68. F. Huang, V.A. Tamma, M. Rajaei, M. Almajhadi, H.K. Wickramasinghe, Measurement of laterally induced optical forces at the nanoscale, Appl. Phys. Lett. **110**, 063103 (2017)

Cite this article as: Jinwei Zeng, Mohammad Kamandi, Mahsa Darvishzadeh-Varcheie, Mohammad Albooyeh, Mehdi Veysi, Caner Guclu, Mina Hanifeh, Mohsen Rajaei, Eric O. Potma, H.Kumar Wickramasinghe, Filippo Capolino, In pursuit of photo-induced magnetic and chiral microscopy, EPJ Appl. Metamat. **5**, 7 (2018)